







Article

# Discovery of RSV-induced BRD4 protein interactions using native immunoprecipitation and parallel accumulation – serial fragmentation (PASEF) mass spectrometry

Morgan Mann <sup>1</sup>, David Roberts <sup>2</sup>, Yanlong Zhu <sup>3,4</sup>, Yi Li <sup>5</sup>, Jia Zhou <sup>5</sup>, Ying Ge <sup>2,3,4</sup>  
and Allan R. Brasier <sup>6\*</sup>

<sup>1</sup> Department of Medicine, Division of Endocrinology, Diabetes, and Metabolism, University of Wisconsin-Madison, Madison, WI, 53705, USA  
<sup>2</sup> Department of Chemistry, University of Wisconsin-Madison, Madison, WI, 53706, USA  
<sup>3</sup> Human Proteomics Program, School of Medicine and Public Health, University of Wisconsin-Madison, Madison, WI, 53705, USA  
<sup>4</sup> Department of Cell and Regenerative Biology, University of Wisconsin-Madison, Madison, WI, 53705, USA  
<sup>5</sup> Department of Pharmacology and Toxicology, University of Texas Medical Branch, Galveston, TX 77550  
<sup>6</sup> Institute for Clinical and Translational Research (ICTR), University of Wisconsin-Madison, Madison, WI, 53705, USA  
\* Correspondence: abrasier@wisc.edu; Tel.: 1-608-263-7371

**Abstract:** Respiratory Syncytial Virus (RSV) causes severe inflammation and airway pathology in children and the elderly by infecting the epithelial cells of the upper and lower respiratory tract. RSV replication is sensed by intracellular pattern recognition receptors upstream of the IRF and NF- $\kappa$ B transcription factors. These proteins coordinate an innate inflammatory response via Bromodomain containing protein 4 (BRD4), a protein that functions as a scaffold for unknown transcriptional regulators. To better understand the pleiotropic regulatory function of BRD4, we examine the BRD4 interactome and identify how RSV infection dynamically alters it. To accomplish these goals, we leverage native immunoprecipitation and Parallel Accumulation – Serial Fragmentation (PASEF) mass spectrometry to examine BRD4 complexes isolated from human alveolar epithelial cells in the absence or presence of RSV infection. In addition, we explore the role of BRD4’s acetyl-lysine binding bromodomains in mediating these interactions by using a highly selective competitive bromodomain inhibitor. We identify 101 proteins that are significantly enriched in the BRD4 complex and are responsive to both RSV-infection and BRD4 inhibition. These proteins are highly enriched in transcription factors and transcriptional coactivators. Among them, we identify members of the AP1 transcription factor complex, a complex important in innate signaling and cell stress responses. We independently confirm the BRD4/ AP1 interaction in primary human small airway epithelial cells. We conclude that BRD4 recruits multiple transcription factors during RSV infection in a manner dependent on acetyl-lysine binding domain interactions. This data suggests that BRD4 recruits transcription factors to target its RNA processing complex to regulate gene expression in innate immunity and inflammation.

**Keywords:** RSV; BRD4; AP-MS; PPI; AP1; Wnt; Innate Immune Response;

## 1. Introduction

Respiratory Syncytial Virus (RSV) is an enveloped, single-stranded, negative-sense RNA virus that infects ciliated epithelial cells in the respiratory tract [1]. RSV infection then spreads to the lower airways, where productive infection of small airway epithelial cells induces rapid activation of the innate immune response, resulting in secretion of pro-inflammatory cytokines [2], anti-viral interferons [3], exosomes [4], and damage-associated patterns [5] that mediate mucous production and leukocytic inflammation [4]. Worldwide, RSV infection is responsible for the plurality of pediatric hospitalizations in children age 5 and younger [6].

31 The innate immune response induced by RSV-infection is mediated by pattern  
32 recognition receptors (PRRs) such as the Toll-like receptors (e.g. TLR3) and Retinoic  
33 acid inducible gene (RIG-I) that monitor the airway lumen and cellular cytoplasm [3,7].  
34 These PRRs recognize double-stranded RNA (dsRNA) and 5'-phosphorylated RNA  
35 as products of effective RSV replication and stimulate the nuclear translocation of the  
36 interferon regulatory factor IRF3 and the various nuclear factor kappa beta (NF-κB)  
37 transcription factors into the nucleus, where they cooperate to induce rapid expression  
38 of pro-inflammatory cytokines and anti-viral interferons [8–10].

39 Upon translocation to the nucleus, NF-κB RelA/p65 interacts with a protein called  
40 Bromodomain containing protein 4 (BRD4), an epigenetic scaffold that mediates the RSV  
41 induced innate immune response [7,11–13]. BRD4 accomplishes this in part through  
42 its tandem bromodomains, which bind acetylated lysine residues on histones and tran-  
43 scription factors like RelA [8]. The resulting BRD4/RelA complex further interacts with  
44 Cyclin-dependent Kinase 9 (CDK9) to form the positive transcription elongation factor  
45 (p-TEFb). p-TEFb in turn initiates transcription via phosphorylation of RNA Polymerase  
46 II (Pol II) complexes paused at the promoters of NF-κB early-intermediate inflammatory  
47 genes [14]. BRD4-dependent transcriptional elongation involves the coordinated actions  
48 of histone acetyl transferases [15,16], cyclin dependent kinases [8] and ubiquitin ligases  
49 [17] that dissociate elongation factors and stimulate polymerase processivity. The mech-  
50 anism by which the transcriptional elongation complex is reprogrammed in the innate  
51 immune response is not well understood.

52 In this study, we apply native immunoprecipitation (IP) of endogenous BRD4 com-  
53 plexes and high-resolution Parallel Accumulation Serial Fragmentation (PASEF)-mass  
54 spectrometry (MS) [18] to address this knowledge gap by examining the BRD4 inter-  
55 actome and its dynamic changes in response to RSV infection. We also measure the  
56 dependence of these interactions on BRD4's bromodomains by perturbing the complex  
57 with the small molecule bromodomain inhibitor, ZL 0454 [19–21]. Our results demon-  
58 strate that BRD4 recruits several inflammation-modulating transcription factors during  
59 RSV infection, including β-catenin of the Wnt-signaling pathway and c-JUN (JUN) and  
60 Fos-Related Antigen 1 (FOSL1) of the AP1 complex. We further show that many of  
61 these transcription factors are sensitive to bromodomain inhibition. Both the interac-  
62 tion with AP1 and its sensitivity to bromodomain inhibition were confirmed in human  
63 small airway epithelial cells (hSAECs). We conclude that RSV dynamically enriches the  
64 BRD4 interactome for pro-inflammatory transcription factors, and that interactions are  
65 dependent on BRD4's bromodomains.

66 **2. Materials and Methods**

67 *2.1. Reagents & Chemicals*

68 The 4-hexylphenylazosulfonate (Azo) used in these experiments was synthesized  
69 in-house as described previously [22,23]. The BRD4 selective BD competitive inhibitor,  
70 ZL 0454, was synthesized as previously described [19,20] and determined to be >99%  
71 pure. All other reagents used for preparation of samples for MS analysis were ACS  
72 grade or higher and purchased from MilliporeSigma unless other-wise noted.

73 *2.2. Virus Preparation and Infection*

74 The human RSV long strain was grown in Hep-2 cells and prepared as described [7,  
75 24]. The viral titer of purified RSV pools was varied from 8 to 9 log PFU/ml, determined  
76 by a methylcellulose plaque assay [25,26]. Viral pools were aliquoted, quick-frozen on  
77 dry ice-ethanol, and stored at -70 °C until used.

78 *2.3. Cell Culture and Treatment*

79 A549 cells (human adenocarcinomic alveolar basal epithelial cells) were obtained  
80 from ATCC and grown in 10% FBS/F12K media (Corning, Corning, NY, USA). Primary  
81 human small airway epithelial cells (hSAECs) were immortalized using human Telom-

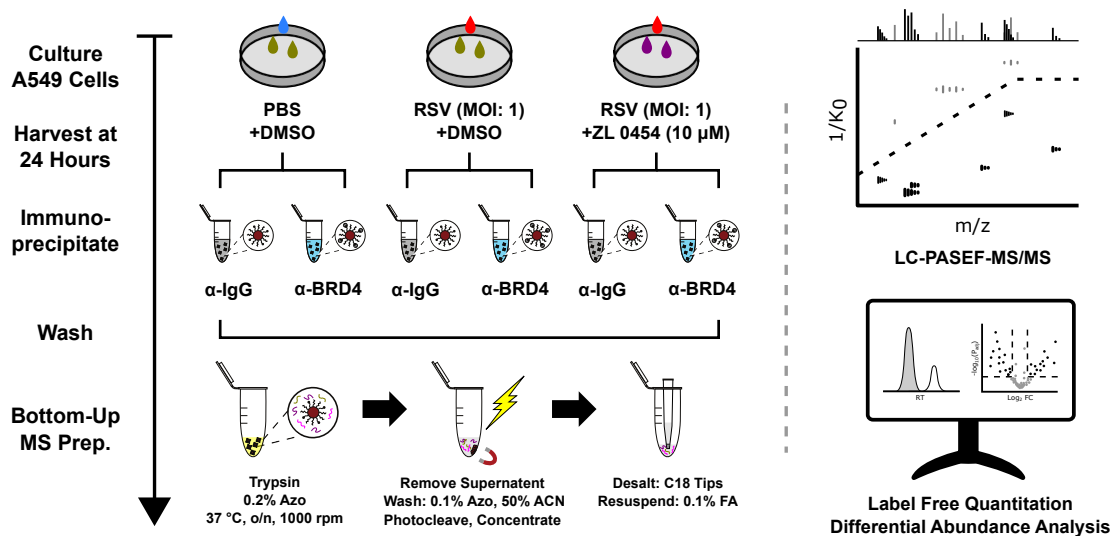


**Figure 1. AP-MS experimental workflow, including sample preparation and data analysis.** In brief, A549 cells were grown to confluence, treated with the bromodomain inhibitor ZL 0454, and infected with RSV. Cells were harvested in a non-denaturing lysis buffer and BRD4 complexes were immunoprecipitated with anti-BRD4 or Isotype Control (IgG) antibodies and protein A magnetic beads. After extensive washing, the isolated proteins were digested on-bead using trypsin in a photocleavable surfactant (Azo) buffer [22,23]. After surfactant removal, the samples were desalted using C18 tips and analyzed via online LC-PASEF-MS/MS. Peptide identification and protein quantification were performed in MaxQuant. Differential abundance analysis was performed using DAPAR and Prostar.

erase/CDK4 as previously described [27,28], and grown in SAGM small airway growth medium (Lonza, Walkersville, MD, USA). All cells were incubated at 37 °C, 5% CO<sub>2</sub> until confluence.

A549 cells were washed twice with Phosphate-buffered Saline (PBS) and exchanged into serum-free F12K media prior to infection with RSV viral particles at a multiplicity of infection (MOI) of 1. Infected A549 cells were harvested at 24 hours post-infection. hSAECs were stimulated with poly(I:C) (MilliporeSigma, Burlington, MA, USA, catalog no. P0913) by introducing the ligand to SAGM media at a final concentration of 50 μg/ml [29]. hSAECs were harvested four hours post-stimulation. The ZL 0454 inhibitor was dissolved in DMSO and added to the relevant cell culture media at a final concentration of 10 μM. The ZL 0454 inhibitor was added 18 hours before infection/stimulation, and to the media during infection/stimulation.

#### 2.4. Protein Extraction and BRD4 Immunoprecipitation

Cells were washed twice with cold PBS before lysis in 500 μL low ionic strength immunoprecipitation buffer (50 mM NaCl, 10 mM HEPES, 1% IGEPAL, 10% Glycerol) with 1 mM Dithiothreitol (DTT) and 1% protease inhibitor cocktail (MilliporeSigma, Burlington, MA, USA, catalog no. P8340) [30]. Lysates were sonicated three times for 10 seconds each time (BRANSON Sonifier 150, setting 4), and centrifuged for 5 minutes at 10,000g, 4 °C. Approximately 3 mg of the supernatant was incubated overnight at 4 °C with 3 μg anti-BRD4 antibody (Cell Signaling, Danvers, MA, USA, catalog no. 13440) for BRD4 immunoprecipitation. A nonspecific isotype control antibody (LSBio, Seattle, WA, USA, catalog no. LS-C149375) was used as a negative control. 30 μL of Protein A magnetic beads (Dynabeads, Invitrogen, Waltham, MA, USA) were added, and the samples were incubated on a rotating mixer for 1 hour at 4 °C. The beads were then separated from the supernatant with a magnetic stand. The beads were washed three times in low ionic strength immunoprecipitation buffer, transferred to a new tube, and washed once more; samples meant for mass spectrometry were washed three additional times in 50 mM NaCl/10 mM HEPES buffer before trypsin digestion.

110 2.5. Trypsin Digestion and Bottom-Up Sample Preparation

111 The magnetic beads were resuspended in 50  $\mu$ L 0.2% 4-hexylphenylazosulfonate  
112 (Azo)/50 mM Ammonium Bicarbonate and reduced with 10 mM DTT at 37 °C for 1 hour.  
113 Freshly prepared iodoacetamide solution (200 mM) was added to a final concentration  
114 of 20 mM, and the samples were incubated in the dark for 30 minutes. The beads were  
115 digested with 1  $\mu$ g Trypsin Gold (Promega, Madison, WI, USA) overnight at 37 °C and  
116 agitation at 1000 rpm. The supernatants were collected, and the beads were further  
117 washed with 100  $\mu$ L 0.1% Azo/50% Acetonitrile. The supernatants and washes were  
118 collected and dried in a vacuum centrifuge to remove the acetonitrile, and resuspended  
119 in 1% formic acid. The samples were then exposed to a mercury lamp (305 nm) for 5  
120 minutes and centrifuged to degrade the Azo and remove byproduct salts. Finally, the  
121 samples were desalted using Pierce C18 tips (Thermo Scientific, Waltham, MA, USA)  
122 and resuspended in 0.1% Formic Acid.

123 2.6. Label-Free Quantitative Proteomics Analysis

124 Desalted peptides (2  $\mu$ L) were loaded and separated on an IonOptiks Aurora  
125 UHPLC column with CSI fitting (Melbourne, Australia) at a flow rate of 0.4  $\mu$ L/minute  
126 and a linear gradient increasing from 0% to 17% mobile phase B (0.1% formic acid in  
127 acetonitrile) (mobile phase A: 0.1% formic acid in water) over 60 minutes; 17% to 25%  
128 from 60 to 90 minutes; 25% to 37% B from 90 to 100 minutes; 37% to 85% B from 100  
129 minutes to 110 minutes; and a 10 minute hold at 85% B before washing and returning to  
130 low organic conditions. The column directly integrated a nanoESI source for delivery of  
131 the samples to the mass spectrometer. MS spectra were captured with a Bruker timsTOF  
132 Pro quadrupole-time of flight (Q-TOF) mass spectrometer (Bruker Daltonics, Billerica,  
133 MA, USA) operating in PASEF mode, with 10 PASEF-MS/MS scans acquired per cycle.  
134 Precursors with charge states ranging from 0 to 5 were selected for fragmentation.

135 Protein identification and quantification were performed using MaxQuant v1.6.17.0  
136 [31,32], with LFQ normalization restricted within sample groups. Four biological repli-  
137 cates with two technical replicates each were used for global label-free quantitation.  
138 Differential protein abundance was established using the "ProStar" and "DAPAR" [33]  
139 R packages for R version 4.0.3 [34]. In brief: protein abundance represented by MS signal  
140 intensity was Log<sub>2</sub>-transformed, and proteins were filtered to remove contaminants, re-  
141 verse identifications, and proteins not quantified in at least 6 out of 8 technical replicates  
142 within at least one sample group. Log<sub>2</sub> intensities were normalized to median of the  
143 global data set, and missing values were imputed via ssla for partially observed values  
144 within a condition, or set to the 2.5% quantile of observed intensities for observations  
145 that were missing entirely within a condition. A limma test was utilized to evaluate  
146 statistical significance based on an FDR-adjusted p-value of less than 0.05. For enrich-  
147 ment of protein in the BRD4 IP over the nonspecific IgG, a Log<sub>2</sub> fold change of 1 or  
148 greater in either direction was used. For comparison of the BRD4 IP between treatments  
149 and biological conditions, the protein abundance was normalized to the abundance of  
150 BRD4 in the sample prior to analysis with ProStar and DAPAR, and a Log<sub>2</sub> fold change  
151 threshold of 0.6 was chosen. P-values were FDR adjusted using the "p.adjust" function  
152 in base R (implementing the Benjamini-Hochberg procedure). Tandem MS spectra were  
153 visualized and plotted using Skyline [35] and the "ggplot2" [36] package for R version  
154 4.0.3. Barplots for protein identifications were generated using the "ggpubr" [37] package  
155 for R version 4.0.3. Venn Diagrams were generated using the "vennDiagram" [38] and  
156 "RColorBrewer" [39] packages for R version 4.0.3.

157 2.7. Gene Ontology and STRING Analysis

158 Proteins identified in BRD4 IP samples but not in the nonspecific IgG pulldown were  
159 submitted to the online PANTHER tool for biological process gene ontology analysis  
160 [40,41]. STRING database analysis [42] was conducted using the list of putative BRD4  
161 interacting proteins that simultaneously displayed 1) increased abundance on the BRD4

complex post-RSV infection and 2) reduced abundance on the RSV-stimulated BRD4 complex post treatment with the ZL 0454 inhibitor. Molecular function gene ontology terms for these proteins were obtained through STRING's built-in analysis functions. For significance, an FDR-adjusted p-value threshold was set at 0.05 for all analyses. GO Dot plots and UpSet plots were generated using the "ggplot2" and "ggupset" [43] packages for R version 4.0.3. Network images were generated in Cytoscape version 3.8.2 [44] using the "stringApp" [45] and "clusterMaker2" [46] plugins.

2.8. Western Blotting

Beads containing immunoprecipitated BRD4 complexes were suspended in 2x Laemli loading buffer and boiled at 95 °C for 5 minutes. The beads were then separated using a magnetic stand, and the supernatants were loaded on a 4-15% Criterion TGX Pre-cast Protein Gel (Biorad, Hercules, CA, USA) for separation. Proteins were transferred to a nitrocellulose membrane using a Trans-Blot Turbo Transfer System (Biorad, Hercules, CA, USA) with a constant voltage of 25 V over 30 minutes. The membrane was blocked for 1 hour using 5% milk powder in Tris-buffered Saline with 0.1% Tween-20 (TBST) and incubated overnight at 4 °C with anti-c-JUN (Cell Signaling, Danvers, MA, USA, catalog no. 9165) or anti-BRD4 antibodies (Cell Signaling, Danvers, MA, USA, catalog no. 13440) diluted 1:1000 in 5% milk powder/TBST. The membrane was washed thoroughly and incubated in VeriBlot IP Detection Reagent (Abcam, Cambridge, UK, catalog no. ab131366) diluted 1:200 in 5% milk powder/TBST. Imaging was performed via chemiluminescent detection using an Azure c500 gel imaging system (Azure Biosystems, Dublin, CA, USA).

3. Results

To investigate the effects of RSV infection on the interactome of BRD4, we utilized native immunoprecipitation and PASEF mass spectrometry to quantify members of the BRD4 complex isolated from A549 human alveolar epithelial cells. A549 cells have been extensively utilized for analysis of airway innate responses, maintain characteristics of type II alveolar cells and are permissive for RSV infection [47,48]. A549 cells were infected with sucrose-cushion purified RSV (long) at a multiplicity of infection (MOI) of 1 for a total duration of 24 hours before harvest. A subset of infected A549 cells were additionally treated with the BRD4 inhibitor ZL 0454 (10 μM) beginning 12 hours before infection. ZL 0454 has been shown to effectively and specifically target the bromodomains of BRD4, with minimal cross-reactivity with other bromodomain proteins [19,21]. Control cells were treated with DMSO, and left uninfected. After 24 hours of viral replication, all cells were harvested according to the workflow presented in Figure 1. Three combinations of biological and treatment conditions resulted: Control-DMSO (CD), RSV-DMSO (RD), and RSV-ZL 0454 (RZ).

3.1. Identification of Putative BRD4 Interactors

Proteins were isolated from harvested cells via immunoprecipitation with an antibody specific to the long isoform of BRD4 (B). A nonspecific isotype control IgG (I) was used as a negative control to screen out contaminants. Accordingly, downstream analyses had 6 experimental groups to consider, resulting from the permutations of the biological conditions ("CD", "RD", "RZ") and pulldown type (BRD4/"B", IgG/"I"). After tryptic digestion, proteomic analysis, and removal of contaminants of reverse identifications, 2874 proteins were identified between all experimental groups. Notably fewer proteins were identified in the ZL 0454 treated samples than in other experimental groups (Figure 2a). We speculate that many proteins and pulldown contaminants had diminished global abundance following the 42-hour transcriptional blockade with ZL 0454, resulting in fewer identifications in these groups.

After filtering to require identification in at least 6 (of 8) technical replicates in one or more biological conditions, this list was reduced to 2580 protein identifications.

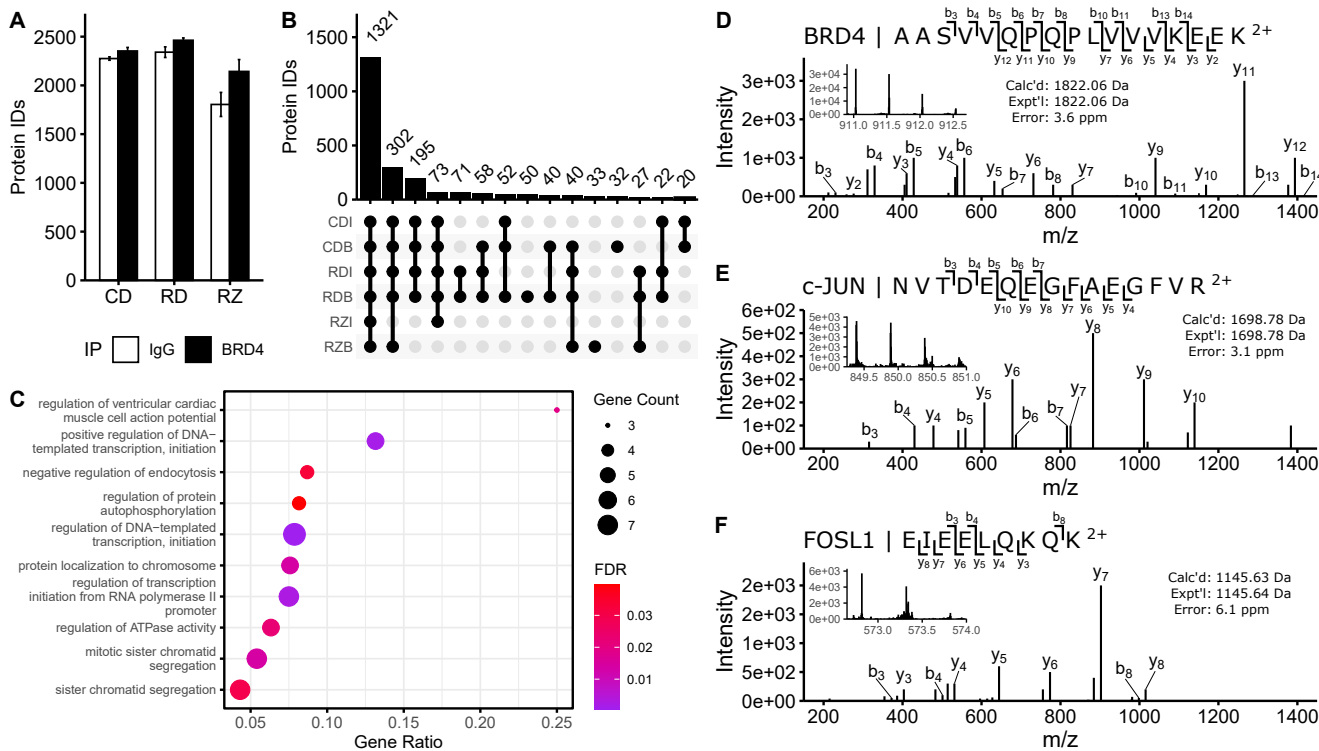


**Figure 2. Identification of immunopurified proteins by PASEF-LC-MS/MS.** (a) Protein identifications per sample group. Bar plot represents the mean of  $n = 8$  biological and technical replicates. (b) UpSet plot of protein identifications shared between sample groups. Protein IDs were filtered to require  $n \geq 6$  identifications per sample group for representation. (c) PANTHER Biological Process GO analysis of proteins identified solely in BRD4 IP groups. Dot size represents the number of identified proteins within a GO group. Gene ratio indicates the fraction of all proteins within the GO group that were identified. Color represents the FDR-adjusted p-value of the GO over-representation test. (d-f) Tandem MS identification of characteristic peptides belonging to BRD4 and notable co-purified proteins. All fragment ion charge states are 1+.

1321 identifications were common to all sample groups, with another 302 identifications missing only in the “RZI” group, and 195 found in all but the “RZ” condition (Figure 2b). Relatively few (188) proteins were identified solely in BRD4 pulldown samples (i.e. not in IgG pulldown controls). These proteins were subjected to PANTHER gene ontology (GO) analysis, with an emphasis on biological process (Figure 2c). The selected proteins were highly enriched for transcriptional regulators and DNA binding proteins, which is consistent with the known roles of BRD4 in Pol II-dependent transcriptional initiation [11,49].

### 3.2. Quantitative Enrichment of BRD4 Interactors

Of the 2580 consensus protein identifications, 1603 were quantifiable in 6 or more technical replicates of at least one experimental group. Under these filters, sample groups demonstrated clear separation in principal component analysis (Figure 3a) with a high degree of pearson correlation within sample groups (Figure 3b). This indicates good reproducibility within groups, as well as markedly different protein abundance profiles between them.

Proteins were evaluated as potential BRD4 interactors based on their relative enrichment in each BRD4 IP over their abundance in the matching IgG control group. (Figure 4). Using a  $\text{Log}_2$  fold change threshold of 1 and an adjusted p-value threshold of 0.05, we identified 230 proteins that were significantly enriched in the Control-DMSO comparison, 186 proteins that were significantly enriched in the RSV-DMSO comparison, and 416 proteins that were significantly enriched in the RSV-ZL 0454 comparison. We speculate that the increased number of enriched proteins in the RSV-ZL condition stems from a

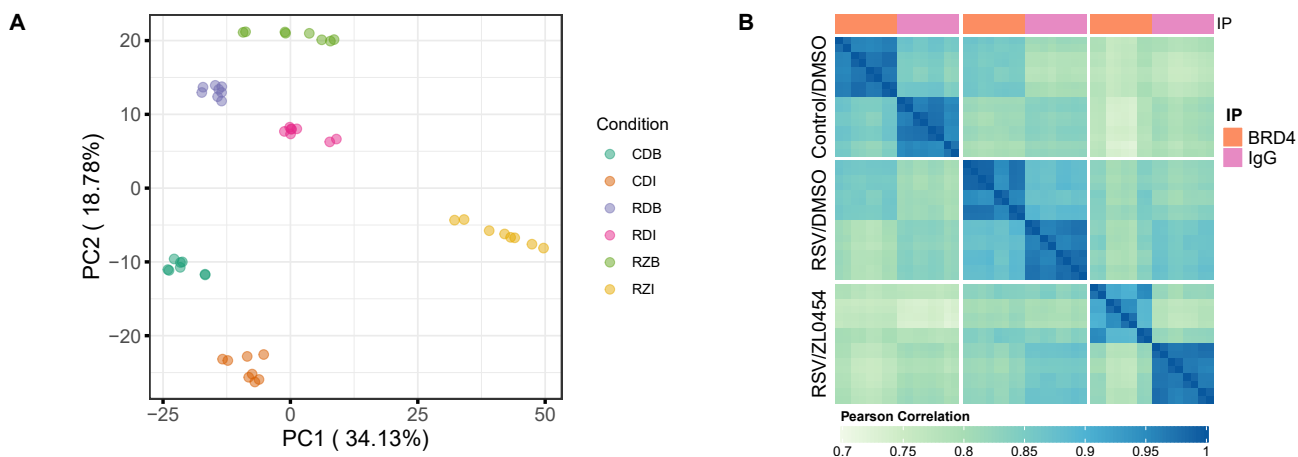


**Figure 3. Sample reproducibility and inter-group variance.** (a) Principal component analysis of per-sample Log<sub>2</sub> protein abundances demonstrates good reproducibility within groups and separation between groups. (b) Heatmap with pearson correlation scores between all samples (biological and technical replicates) in the experiment.

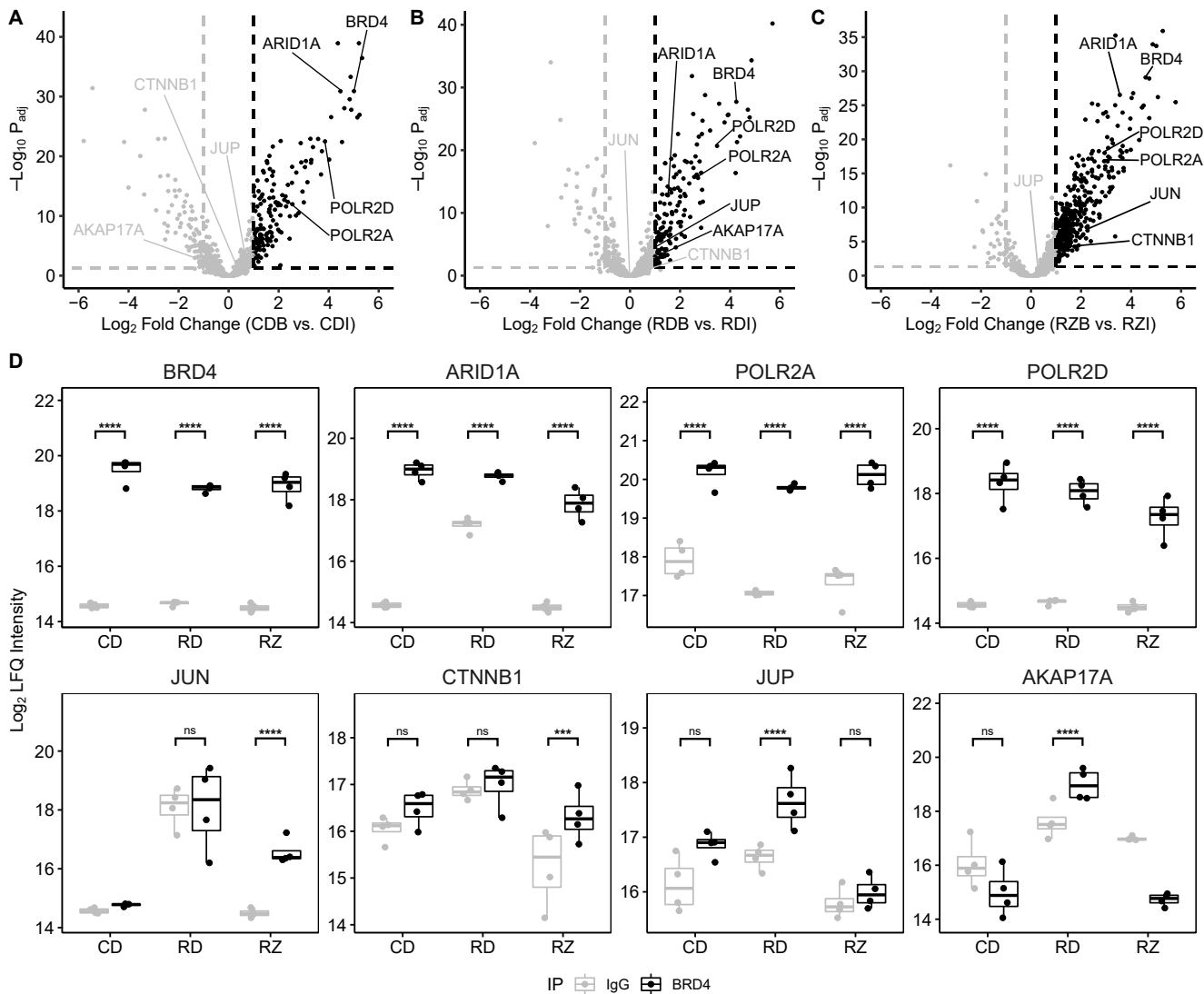


**Figure 4. Potential BRD4 interactors are enriched over the IgG antibody.** (a-c) Volcano plots demonstrating fold change enrichment of the BRD4 IP over the IgG IP in each biological condition. (d) Boxplots demonstrate enrichment of BRD4 and notable co-purified proteins in each biological condition. Boxplots represent n=4 biological replicates per experimental group. Each data point represents the mean of n=2 technical replicates. \*\*\**P*<sub>adj</sub> < 0.001, \*\*\*\**P*<sub>adj</sub> < 0.0001.

reduced background protein abundance following ZL 0454 transcriptional blockade. In support of this conclusion, we note that many proteins quantified in IgG pulldowns display differential abundance between biological conditions. Between all three comparisons, 557 unique proteins were significantly enriched and were categorized as potential interactors. Among these proteins, we identify ARID1A, and multiple subunits of the Pol II and Mediator complexes – all known interactors with BRD4 [30]. Additionally, we identify multiple transcription factors, ATPases, splicing factors, ribosomal proteins, and related eukaryotic initiation factors (**Figure 4d**). These enriched proteins are suggestive for additional roles of the BRD4 complex in mRNA processing and translation.

We note that the canonical BRD4 interactors, CDK9 and NF- $\kappa$ B RelA, are not flagged as potential interactors in this analysis, despite the fact that we identified both proteins during our experiment. In the case of RelA, we observed a high abundance of the protein in both the "RDI" and "RDB" sample groups, and accordingly enrichment could not be established (**Supplementary Material Figure S1a**). This likely reflects an increase in the protein's global abundance that was captured on the nonspecific IP. CDK9, in contrast, was not reliably quantified (fewer than 6 intensity values in any given sample group) and thus was omitted from further analysis. Interestingly, we were able to reliably identify and quantify the enrichment of Cyclin-dependent Kinase 12 (CDK12) (**Figure 5d & Supplementary Material Figure S2d**), which functions in a highly similar manner to CDK9 [50,51].

### 3.3. RSV-induced BRD4 Protein Interactions

Once we had identified these 557 potential BRD4 interactors, we proceeded to examine how RSV infection altered their relative abundance within the BRD4 complex. To correct for differences in BRD4 abundance by treatment, protein abundances in the pulldowns were normalized to that of BRD4. The resulting  $\text{Log}_2(\text{Protein}/\text{BRD4})$  ratios were then compared between the biological conditions to identify differential membership in the BRD4 complex. For this purpose, an absolute  $\text{Log}_2$  fold change threshold of 0.6 (corresponding to a positive 1.5 fold change in the usual scale) and an FDR-adjusted p-value threshold of 0.05 were set. Under these criteria, RSV infection resulted in a significant increase to the  $\text{Log}_2(\text{Protein}/\text{BRD4})$  ratio of 272 proteins (**Figure 5a**); 174 of these proteins displayed an absolute 2-fold change ( $\text{Log}_2$  fold change  $> 1$ ) in abundance or greater. In a manner similar to the list of putative interactors, we found that RSV-infection significantly increased the relative abundance of transcription factors and coactivators, ATPases, splicing factors, cytoskeleton binding proteins, and numerous proteins associated with translational machinery (**Supplementary Material Figure S3**). In particular, we highlight the recruitment of multiple members of the AP1 transcription factor complex (i.e. c-JUN, FOSL1), as well as several associated proteins (e.g. MAP4K4, NACA) (**Figure 6a**). AP1 is a ubiquitous transcription factor that participates in the activation of pro-inflammatory cytokines [52–54]. Mitogen-activated protein kinase kinase kinase 4 (MAP4K4) and Nascent polypeptide associated complex subunit alpha (NACA) also contribute to AP1 via activation of the Jun N-terminal kinase [55] and stabilization of c-JUN homodimers [56], respectively. This interaction suggests that BRD4 and AP1 cooperate to initiate transcription of pro-inflammatory cytokines.

In contrast to the proteins with increased relative abundance, only 35 proteins displayed a significant reduction ( $\text{Log}_2$  fold change  $< -0.6$ ) in membership to the BRD4 complex post RSV infection. These proteins were enriched for components of the nuclear pore complex and mRNA export machinery, as well as core cell cycle regulators (**Supplementary Material Figure S4**).

### 3.4. Inhibitor-sensitive BRD4 Interactors

The effect of bromodomain inhibition on the RSV-stimulated BRD4 complex was similarly determined by comparing the BRD4-normalized "RZB" and "RDB" groups (**Figure 5b**). In this contrast, we observed 81 proteins that significantly increased their

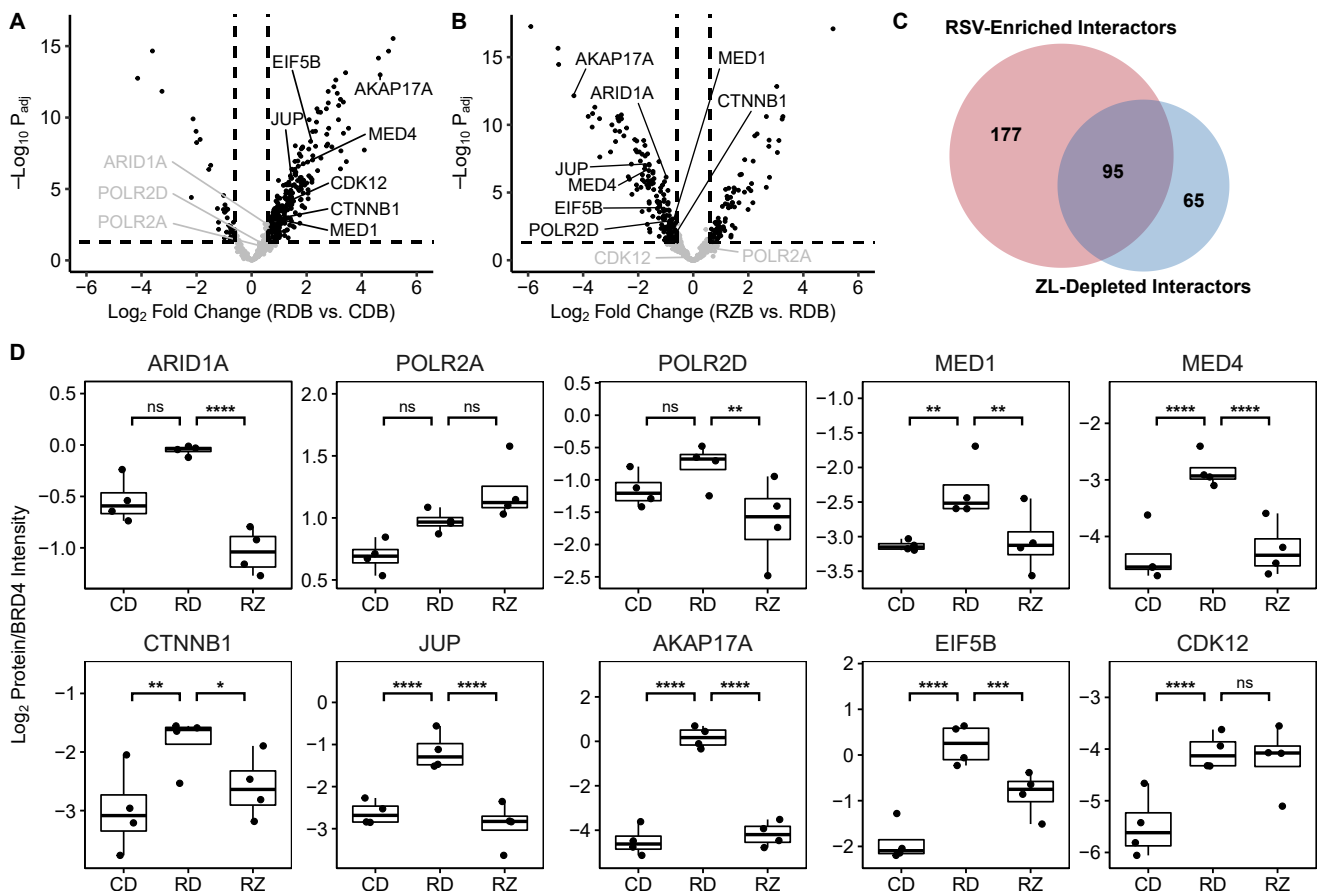


**Figure 5. RSV-infection induces bromodomain-sensitive BRD4 interactions.** (a) Volcano plot demonstrating fold change enrichment of BRD4 interactors induced by RSV-infection. (b) Volcano plot demonstrating fold change alterations to the RSV-stimulated BRD4 complex when treated with ZL 0454. (c) Venn diagram illustrates overlap between RSV-enriched interactions and ZL 0454-depleted interactions. (d) Boxplots demonstrate relative abundance of notable proteins in the BRD4 complex. Boxplots represent n=4 biological replicates per experimental group. Each data point represents the mean of n=2 technical replicates. \* $P_{adj} < 0.05$ ; \*\* $P_{adj} < 0.01$ ; \*\*\* $P_{adj} < 0.001$ ; \*\*\*\* $P_{adj} < 0.0001$ .

membership in the BRD4 complex, as well as 160 that significantly decreased their relative abundance. 51 of these proteins displayed a Log<sub>2</sub> fold change exceeding 1, and 103 displayed a Log<sub>2</sub> fold change less than -1. Interestingly, we observed that treating A549 cells with 10  $\mu$ M ZL 0454 resulted in a reversal to many RSV-stimulated changes (Figure 5c); 95 proteins that had significantly increased abundance on the BRD4 complex following RSV-infection were significantly reduced following ZL 0454 treatment. 6 proteins displayed the opposite trend, with reduced abundance in the RSV-stimulated complex that was restored by bromodomain inhibition. This subset of differentially represented proteins is highly enriched in transcriptional coactivators, nuclear pore constituents, and mRNA splicing factors (Figure 7). This includes the AP1 complex member c-JUN, as well as the associated protein NACA. Notably, FOSL1 and MAP4K4 relative abundances were not significantly reduced by bromodomain inhibition, and c-JUN relative abundance remained above baseline, suggesting that BRD4 may interact with both AP1 c-JUN homodimers and AP1 JUN/FOSL1 heterodimers. CDK12 was likewise unaffected by bromodomain inhibition, which is consistent with the interaction mechanism of the related CDK9 protein, which interacts with BRD4 via its C-terminal domain rather than its bromodomains [57].

We also observe that BRD4 interacts with members of the E-cadherin (e.g.  $\beta$ -catenin/CTTNB1,  $\gamma$ -Catenin/JUP) complex in an RSV- and bromodomain inhibitor-specific manner. This complex is enriched in cell-cell junctions and regulates gene

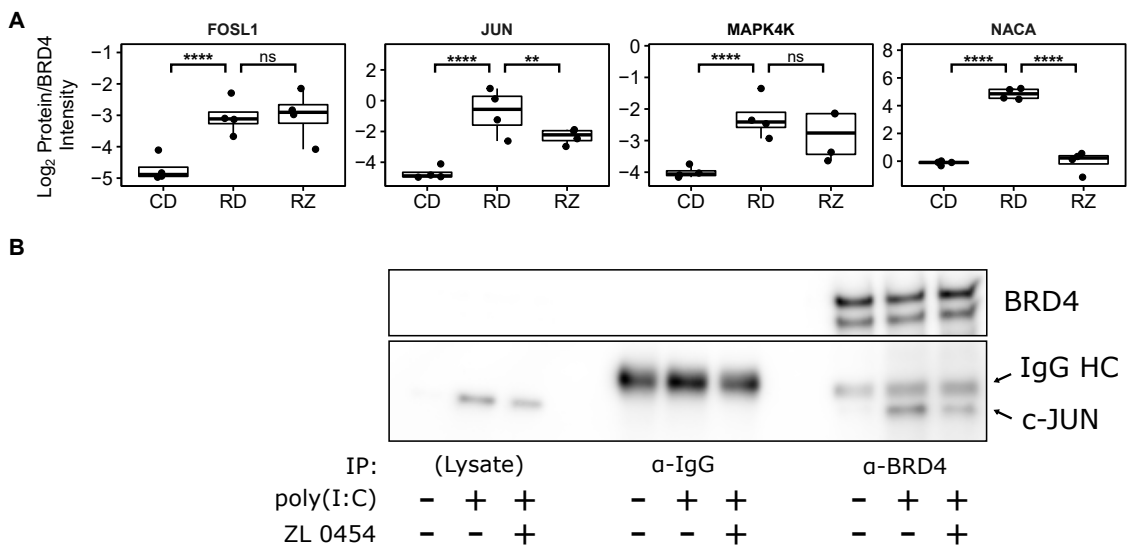


**Figure 6. BRD4 recruits the AP1 transcription factor complex during RSV-infection.** (a) Protein abundance boxplots of AP1 complex members and related proteins. Boxplots represent n=4 biological replicates per experimental group. Each data point represents the mean of n=2 technical replicates. \*\* $P_{adj} < 0.01$ ; \*\*\*\* $P_{adj} < 0.0001$ . (b) Confirmatory western blot, demonstrating that TLR3-induced inflammation in hSAECs triggers the BRD4/c-JUN interaction in a bromodomain-sensitive manner. (+/-) indicates the presence or absence of the respective compound in a given lane. "IgG HC" refers to the anti-BRD4 antibody heavy chain.

expression through direct and indirect mechanisms.  $\beta$ -catenin is known to indirectly interact with NF- $\kappa$ B RelA in a tissue and stimulus-specific manner that can either up-regulate or downregulate NF- $\kappa$ B signalling. Similarly,  $\beta$ -catenin has been observed to interact with AP1 [58], and AP1 is known to cooperate with RelA [59]. This suggests that NF- $\kappa$ B, AP1, and Wnt signalling converge on BRD4 to regulate gene expression, and that bromodomain inhibition can interrupt this process.

### 3.5. Validation of the BRD4/AP1 Interaction

To confirm the discovered interaction with AP1 and its sensitivity to the small molecule bromodomain inhibitor ZL 0454, we immunoprecipitated BRD4 complexes from human small airway epithelial cells (hSAECs). hSAECs are telomerase-immortalized human small airway cells that maintain stable epithelial morphology in monoculture, and reproduce both genomic and proteomic signatures of primary cells without early senescence [4]. hSAECs were treated with 10  $\mu$ M ZL 0454, and stimulated with the specific Toll-like Receptor 3 (TLR3) ligand poly(I:C) to induce inflammation similar to that of RSV infection [60,61]. Detection via western blot and a specific antibody for c-JUN confirmed that inflammation induces an interaction between BRD4 and the AP1 subunit c-JUN (Figure 6b). This experimental result also confirmed that this interaction was sensitive to bromodomain inhibition with ZL 0454.

## 4. Discussion

Respiratory syncytial virus is a common human pathogen and the single largest cause of pediatric hospitalization in the United States [6]. As a consequence of RSV replication in the lungs and airways, innate inflammation triggered in the airway epithelium plays a significant role in the progress and resolution of the disease. The innate inflammatory response proceeds largely through the actions of NF- $\kappa$ B [8] and IRF [7] transcription factors, which converge on BRD4, an epigenetic scaffold that interacts with transcription factors and cyclin-dependent kinases to enable Pol II-dependent transcriptional initiation. Previous works have identified over 250 high confidence members of the basal BRD4 interactome [30], including members of the SWI/SNF, DNA-directed Pol

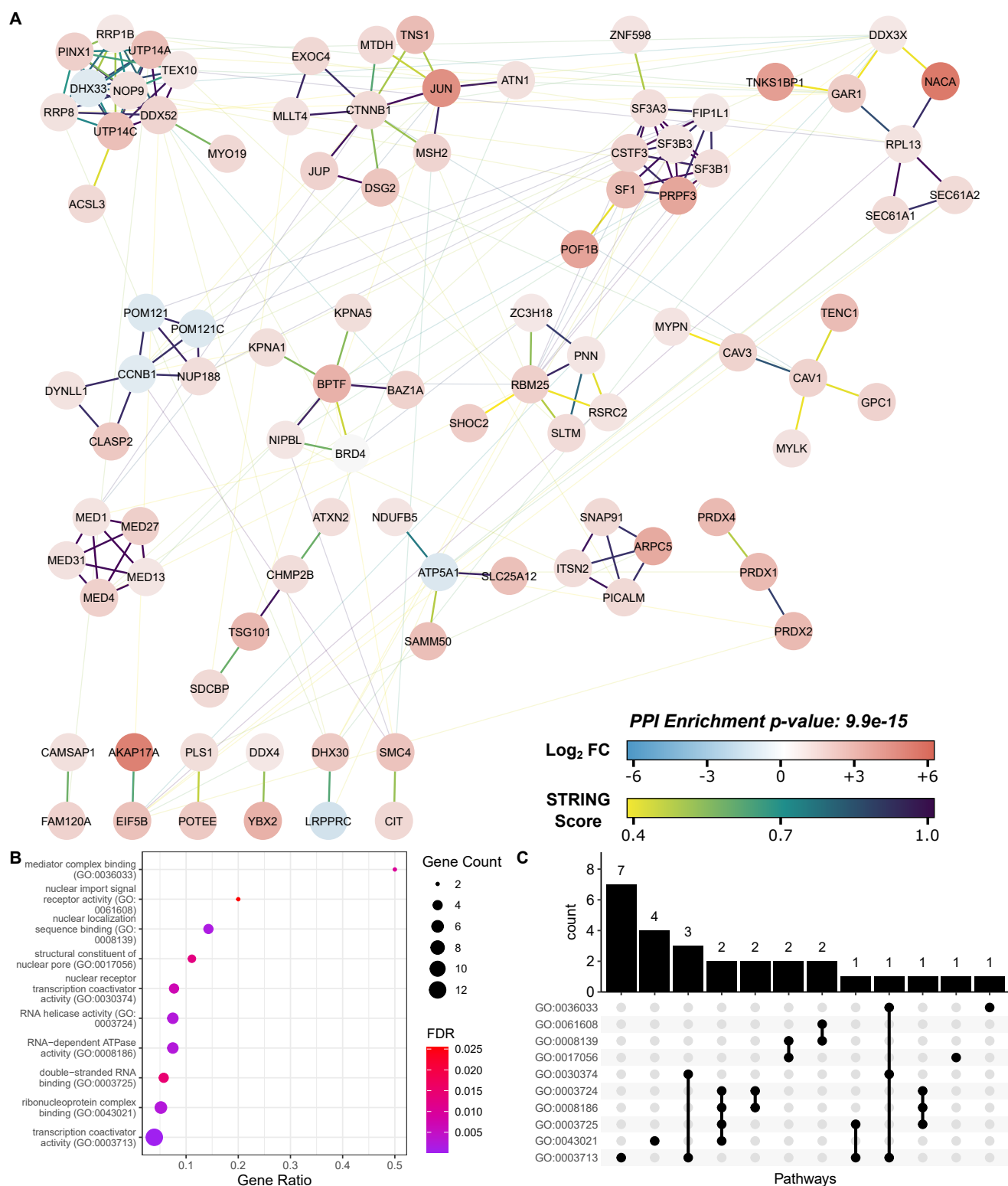


**Figure 7. STRING analysis of RSV-inducible and bromodomain-sensitive BRD4 interactors.** (a) Cytoscape network visualization of 101 RSV-inducible and bromodomain-dependent BRD4 interactors. Node color represents the RSV-inducible Log<sub>2</sub> fold change. Edge color is keyed to the STRING score and represents interaction confidence. Low confidence interactions (STRING score < 0.4) and nodes without interactions are omitted. (b) STRING Molecular Function GO Analysis. Dot size represents the number of identified proteins within a GO group. Gene ratio indicates the fraction of all proteins within the GO group that were identified. Color represents the FDR-adjusted p-value of the GO over-representation test. (c) UpSet plot of proteins with shared GO terms. Each bar represents the number of proteins shared between marked pathways.

II complex, ribonucleoprotein, AP-2 adaptor, and spliceosomal complexes. Building on that foundation, we have utilized high-resolution, PASEF mass spectrometry to identify 557 interactors over three biological conditions in A549 cells, and 272 interactors that are enriched on the RSV-stimulated BRD4 complex. These interactions are consistent with the previous body of work, and demonstrate that viral infection reorders the interactome of BRD4, enriching it for transcription and splicing factors, as well as kinases, ATPases, and translational machinery. We also demonstrate that a significant proportion of these interactions are sensitive to bromodomain inhibition, indicating that they are facilitated either directly or through downstream feedback signaling by BRD4's acetyl-lysine binding activity. STRING network analysis and molecular function GO enrichment indicate that these proteins are highly associated with nuclear pore function, RNA binding, and transcriptional coactivator activity.

4.1. PASEF Mass Spectrometry as a High-Resolution Tool for Dynamic Interactome Analysis

Mass spectrometry-based shotgun proteomics has been widely applied for the discovery of protein interactions via affinity purification samples [62]. While often considered the gold-standard for modern interactome studies, Affinity Purification Mass Spectrometry (AP-MS) often fails to identify low abundance interaction partners [63], despite the physiological importance that they can play. A variety of strategies have been implemented to improve quantitation of low-abundance peptides [64,65], but all come with trade-offs in the experimental workflow or the efficiency of protein identifications. In this study, we utilized PASEF mass spectrometry [18], which implements a trapped ion mobility spectrometer to simultaneously exclude non-peptide contaminants from MS acquisition, separate isobaric precursors, and focus ions to improve sensitivity and throughput. This approach enabled us to deeply examine the interactome of endogenous BRD4, despite the low relative abundance of many interactors and the low cellular abundance of BRD4 itself.

Over three biological conditions, we quantified over 1600 proteins and validated 557 (35%) as potential BRD4 interactors. These proteins were identified with high-quality tandem mass spectra, and quantified based on technical duplicates of 4 biological replicates per biological condition and per antibody. Together with the data's consistency with previous works [30,66] and our independent validation of the BRD4/AP1 interaction in hSAECs, this argues that our data is of high quality, and that our conclusions on RSV-stimulated and bromodomain-dependent interactions are valid.

4.2. BRD4 Recruits Inflammation-modulating Transcription Factors during RSV Infection

During the process of viral infection, NF- $\kappa$ B RelA traffics to the nucleus and interacts with BRD4, CDK9 and other components of the positive transcription elongation factor (p-TEFb) [7]. The resulting complex phosphorylates Pol II, releasing it from a paused state on the promoters of pro-inflammatory and anti-viral genes [14]. This process results in a rapid and robust innate immune response which helps to reduce viral proliferation and recruit the cellular immune response. However, many NF- $\kappa$ B dependent genes experience delayed activation in response to inflammatory stimulus, and other genes with NF- $\kappa$ B binding sites remain inactive throughout the process [67–69], indicating complex transcriptional and epigenetic regulation. It is currently unclear how BRD4 circumvents these barriers.

To address this information gap, we conducted what is, to our knowledge, the first study to examine BRD4's dynamic interactome in an unbiased manner. Previous studies have either focused on the basal interactome [30,66,70], or utilized highly-targeted assays to study individual interactions [71,72], such as the interaction between BRD4 and RelA [7]. This unbiased approach enabled us to discover novel, RSV-induced BRD4 interactions with transcription factors from multiple pathways. These included the AP1 transcription factor (e.g. c-JUN, FOSL1), and both  $\beta$ -catenin and Junction Plakoglobin, of the Wnt-signalling pathway. Other transcription factors are also enriched in this

387 fashion, including DEAD-Box Helicase 3 (DDX3X), Metadherin (MTDH), and multiple  
388 members of the mediator complex (e.g. MED1, MED4, MED13, MED31). Remarkably,  
389 all of these proteins either modulate NF- $\kappa$ B [73–76] or directly facilitate the expression  
390 of pro-inflammatory cytokines and antiviral genes [54].

391 AP1 is a ubiquitous family of transcription factors composed of JUN-family ho-  
392 modimers and JUN/FOS-family heterodimers [77]. Multiple paralogs of both JUN and  
393 FOS exist and contribute to significant diversity in the effect and mechanisms of AP1  
394 complexes. In the context of viral and TLR3-dependent inflammation, AP1 activates  
395 expression of numerous pro-inflammatory cytokines, including IL-6, IL-8, CD38, and  
396 TNF [54]. These genes are also highly induced via NF- $\kappa$ B, and interestingly, many NF- $\kappa$ B  
397 dependent genes also present AP1 binding sites and require the AP1 subunit c-JUN for  
398 efficient transcription [78].

399 Wnt-signaling through  $\beta$ -catenin is also associated with inflammation, but in a  
400 more nuanced fashion; Wnt/ $\beta$ -catenin can either repress or co-activate NF- $\kappa$ B-dependent  
401 inflammation via interactions with RelA in a cell-type and stimulus specific manner  
402 [79,80]. In some cases, NF- $\kappa$ B may serve as a coactivator for genes under the control of  
403 the Wnt pathway and drive aberrant expression of stem cell signature genes, which is  
404 observed to contribute to tumorigenesis [81]. Notably, interactions between  $\beta$ -catenin  
405 and RelA have been observed to be indirect; these two proteins did not physically  
406 associate in the absence of cell extracts [82]. Our results suggest that BRD4 may be a  
407 mediator of this association.

408 Finally, interactions have also been observed between  $\beta$ -catenin and AP1, and  
409  $\beta$ -catenin binding sites are often enriched with AP1 binding sites [83,84]. c-JUN was  
410 reported to physically associate with  $\beta$ -catenin via interfaces at its N-terminus and  
411 DNA-binding domain [58]. Interestingly, this interaction promoted Cyclin D1 and c-Myc  
412 gene expression in a manner completely independent of AP1 binding sites. Altogether,  
413 our data suggests that the BRD4 complex integrates signals from the NF- $\kappa$ B, AP1, and  
414 Wnt pathways during RSV-infection and facilitates crosstalk between them.

415 *4.3. RSV-induced Interactions are Bromodomain-dependent*

416 Small molecule bromodomain-and-extra-terminal (BET) inhibitors competitively  
417 occupy the bromodomains of BRD4 and related proteins, and have been used extensively  
418 over the last decade to disrupt bromodomain mediated transcriptional activity and probe  
419 related physiology [85,86]. In the context of airway inflammation, BET inhibitors have  
420 been demonstrated to block BRD4-mediated expression of pro-inflammatory cytokines  
421 and interferons, while preventing downstream airway remodeling via the epithelial-  
422 to-mesenchymal transition (EMT) [20]. Classically, BRD4 inhibitors suffer from low-  
423 specificity and dose-limiting toxicity [86]. In this study, we utilize the ZL 0454 BET  
424 inhibitor discovered by our group. In previous studies, we showed that ZL 0454 se-  
425 lectively binds to both BRD4 bromodomains with nanomolar affinity, and displaces  
426 acetylated histones. In contrast to nonselective BET-isoform inhibitors, ZL0454 does not  
427 produce detectable toxicity in cell culture or in vivo [19]. These unique properties enabled  
428 us to probe the bromodomain-dependence of numerous RSV-induced BRD4 interactions  
429 and provide insight into the mechanisms of BRD4-mediated innate inflammation.

430 Of the 227 BRD4 interactors that were recruited to the BRD4 complex during RSV-  
431 infection, we observe that 95 ( 42%) are disrupted to some degree by treatment with  
432 ZL 0454, including most of the transcription factors described in the earlier section (e.g.  
433 c-JUN, CTNNB1, JUP, DDX3X, MTDH). In particular, we note that the recruitment of  $\beta$ -  
434 catenin and  $\gamma$ -catenin, as well as that of the mediator complex, is completely abrogated by  
435 competition for the acetyl lysine binding pocket of the BRD4 bromodomains. Considered  
436 together with the prominent role that  $\beta$ - and  $\gamma$ -catenin play in the EMT [87], this suggests  
437 that BET inhibitors may block airway remodeling by interfering with BRD4-mediated  
438 Wnt-signaling.

In addition to the catenins, we also observe partial depletion of members of the AP1 complex. In the case of c-JUN, we observe a nearly 3-fold reduction in response to bromodomain inhibition. Likewise, NACA – which is reported to stabilize c-JUN homodimers [56] – is completely displaced from the BRD4 complex by ZL 0454. Despite this finding, we observed no reduction to the AP1 complex member FOSL1, with which c-JUN can alternatively form a heterodimer [77]. Further investigation will be required to confirm the exact nature of the BRD4/ AP1 interaction, but these results suggest that BRD4 may recruit both AP1 homodimers and AP1 heterodimers via distinct interaction surfaces during RSV-infection.

4.4. *Non-transcriptional Roles of Dynamic BRD4 Interactors*

Our discussion has focused primarily on RSV-induced protein interactors with transcriptional activity, but we also observe RSV-induced interactors with roles in other contexts, such as mRNA splicing (e.g. SF1, SF3A3, SF3B1, AKAP17A) [88,89], translation (e.g. RPS17, EIF3D, EIF5B) [90,91], protein folding (e.g. CCT5, CCT6A, CCT8) [92], and endoplasmic reticulum (ER)-targeting (e.g. SEC61A1, SEC61B) [93]. That is, we observe that BRD4 associates with protein complexes representing downstream elements of the central dogma of molecular biology. This, in turn, opens the possibility that BRD4 may funnel the products of activated genes into downstream processing complexes, thereby facilitating accelerated alternative splicing and translation, before transport to the ER for additional processing and secretion. In support of this, we note that alternative splicing can often be coupled to transcription [94], and splicing factors have been observed to interact with ribosomes and regulate translation [95,96]. While intriguing, BRD4's role in these contexts has not been explored in the literature. Our data will therefore serve as a useful starting point for investigation into the potential post-transcriptional roles of BRD4.

5. **Conclusions**

In summary, using an unbiased affinity purification- mass spectrometry approach we identify dynamic, bromodomain-dependent changes to the BRD4 interactome in response to RSV infection. Taking advantage of a high-resolution mass spectrometer equipped with a trapped ion mobility spectrometer as a filter, we deeply interrogate the BRD4 interactome, identifying over 500 potential BRD4 interactors and over 270 RSV-induced changes to the interactome. This data will provide new hypotheses for understanding the pleiotropic role of BRD4 in the innate immune response and in viral infection.

**Supplementary Materials:** The following are available online at <https://www.mdpi.com/1999-4915/1/1/0/s1>, Figure S1: NF-κB RelA and Cyclin-dependent Kinase 9 (CDK9) are identified but not qualified as BRD4 interactors., Figure S2: Tandem MS of characteristic peptides belonging to notable proteins in the main text. Figure S3: STRING analysis of RSV-inducible BRD4 interactors. Figure S4: STRING analysis of RSV-reduced BRD4 Interactors. Table S1: Enrichment of potential BRD4 interactors over IgG. Table S2: Relative enrichment of BRD4 interactors between biological conditions. Table S3: Maxquant output of all experimentally identified proteins and associated quantitation.

**Author Contributions:** Conceptualization, M.M. and A.B.; software, M.M.; validation, M.M.; formal analysis, M.M. and Y.Z.; investigation, M.M.; resources, Y.L., J.Z., and Y.G.; writing—original draft preparation, M.M.; writing—review and editing, M.M., D.R., Y.Z., Y.L., Y.G., and A.B.; visualization, M.M.; supervision, D.R., Y.Z., Y.G., and A.B.; project administration, Y.G. and A.B.; funding acquisition, A.B. All authors have read and agreed to the published version of the manuscript.

**Funding:** This work was partially supported by NIH grants AI062885 (ARB, RPG) and NCATS UL1TR002373 (ARB). The funders had no role in the design of the study; in the collection, analyses, or interpretation of data; in the writing of the manuscript, or in the decision to publish the results.

**Data Availability Statement:** All data contained within this manuscript are available upon reasonable request of the corresponding author. The mass spectrometry proteomics data have been deposited to the ProteomeXchange Consortium via the PRIDE [97] partner repository with the dataset identifier [To be added when fully uploaded].

**Acknowledgments:** The authors would like to acknowledge the UW-Madison Human Proteomics Program Mass Spectrometry Facility (initially funded by the Wisconsin partnership funds) for support in obtaining mass spectrometry data and NIH S10OD018475 for the acquisition of ultra-high resolution mass spectrometer for biomedical research. We would also like to thank Bruker for providing the timsTOF Pro mass spectrometer that was used in the study for the collection of all mass spectrometry data.

**Conflicts of Interest:** The University of Wisconsin–Madison has filed a patent application “PHOTO-CLEAVABLE SURFACTANTS FOR TOP-DOWN AND BOTTOM-UP PROTEOMICS” for the use of Azo in proteomics applications.

**Abbreviations**

The following abbreviations are used in this manuscript:

RSV	Respiratory Syncytial Virus
BRD4	Bromodomain containing protein 4
Pol II	RNA Polymerase II
AP-MS	Affinity Purification Mass Spectrometry
PASEF	Parallel accumulation - Serial fragmentation
CD	Control - DMSO
RD	RSV - DMSO
RZ	RSV - ZL 0454
CDI	Control - DMSO - IgG Immunoprecipitation
CDB	Control - DMSO - BRD4 Immunoprecipitation
RDI	RSV - DMSO - IgG Immunoprecipitation
RDB	RSV - DMSO - BRD4 Immunoprecipitation
RZI	RSV - ZL 0454 - IgG Immunoprecipitation
RZB	RSV - ZL 0454 - BRD4 Immunoprecipitation

**References**

1. Eiland, L.S. Respiratory syncytial virus: diagnosis, treatment and prevention. *J Pediatr Pharmacol Ther* **2009**, *14*, 75–85. Type: Journal Article, doi:10.5863/1551-6776-14.2.75.

2. Zhang, Y.; Luxon, B.A.; Casola, A.; Garofalo, R.P.; Jamaluddin, M.; Brasier, A.R. Expression of respiratory syncytial virus-induced chemokine gene networks in lower airway epithelial cells revealed by cDNA microarrays. *J Virol* **2001**, *75*, 9044–58. Type: Journal Article, doi:10.1128/JVI.75.19.9044-9058.2001.

3. Liu, P.; Jamaluddin, M.; Li, K.; Garofalo, R.P.; Casola, A.; Brasier, A.R. Retinoic acid-inducible gene I mediates early antiviral response and Toll-like receptor 3 expression in respiratory syncytial virus-infected airway epithelial cells. *J Virol* **2007**, *81*, 1401–11. Type: Journal Article, doi:10.1128/JVI.01740-06.

4. Zhao, Y.; Jamaluddin, M.; Zhang, Y.; Sun, H.; Ivanciuc, T.; Garofalo, R.P.; Brasier, A.R. Systematic Analysis of Cell-Type Differences in the Epithelial Secretome Reveals Insights into the Pathogenesis of Respiratory Syncytial Virus-Induced Lower Respiratory Tract Infections. *J Immunol* **2017**, *198*, 3345–3364. Type: Journal Article, doi:10.4049/jimmunol.1601291.

5. Hosakote, Y.M.; Brasier, A.R.; Casola, A.; Garofalo, R.P.; Kurosky, A. Respiratory Syncytial Virus Infection Triggers Epithelial HMGB1 Release as a Damage-Associated Molecular Pattern Promoting a Monocytic Inflammatory Response. *J Virol* **2016**, *90*, 9618–9631. Type: Journal Article, doi:10.1128/JVI.01279-16.

6. Group, P.E.R.f.C.H.P.S. Causes of severe pneumonia requiring hospital admission in children without HIV infection from Africa and Asia: the PERCH multi-country case-control study. *Lancet* **2019**, *394*, 757–779. Type: Journal Article, doi:10.1016/S0140-6736(19)30721-4.

7. Tian, B.; Yang, J.; Zhao, Y.; Ivanciuc, T.; Sun, H.; Garofalo, R.P.; Brasier, A.R. BRD4 Couples NF- $\kappa$ B/RelA with Airway Inflammation and the IRF-RIG-I Amplification Loop in Respiratory Syncytial Virus Infection. *J Virol* **2017**, *91*. Type: Journal Article, doi:10.1128/JVI.00007-17.

8. Brasier, A.R.; Tian, B.; Jamaluddin, M.; Kalita, M.K.; Garofalo, R.P.; Lu, M. RelA Ser276 phosphorylation-coupled Lys310 acetylation controls transcriptional elongation of inflammatory cytokines in respiratory syncytial virus infection. *J Virol* **2011**, *85*, 11752–69. Type: Journal Article, doi:10.1128/JVI.05360-11.

9. Schneider, W.M.; Chevillotte, M.D.; Rice, C.M. Interferon-stimulated genes: a complex web of host defenses. *Annu Rev Immunol* **2014**, *32*, 513–45. Type: Journal Article, doi:10.1146/annurev-immunol-032713-120231.
10. Ivashkiv, L.B.; Donlin, L.T. Regulation of type I interferon responses. *Nat Rev Immunol* **2014**, *14*, 36–49. doi:10.1038/nri3581.
11. Devaiah, B.N.; Singer, D.S. Two faces of brd4: mitotic bookmark and transcriptional lynchpin. *Transcription* **2013**, *4*, 13–7. Type: Journal Article, doi:10.4161/trns.22542.
12. Dey, A.; Chitsaz, F.; Abbasi, A.; Misteli, T.; Ozato, K. The double bromodomain protein Brd4 binds to acetylated chromatin during interphase and mitosis. *Proc Natl Acad Sci U S A* **2003**, *100*, 8758–63. Type: Journal Article, doi:10.1073/pnas.1433065100.
13. Hajmirza, A.; Emadali, A.; Gauthier, A.; Casasnovas, O.; Gressin, R.; Callanan, M.B. BET Family Protein BRD4: An Emerging Actor in NF $\kappa$ B Signaling in Inflammation and Cancer. *Biomedicines* **2018**, *6*. Type: Journal Article, doi:10.3390/biomedicines6010016.
14. Tian, B.; Zhao, Y.; Kalita, M.; Edeh, C.B.; Paessler, S.; Casola, A.; Teng, M.N.; Garofalo, R.P.; Brasier, A.R. CDK9-dependent transcriptional elongation in the innate interferon-stimulated gene response to respiratory syncytial virus infection in airway epithelial cells. *J Virol* **2013**, *87*, 7075–92. Type: Journal Article, doi:10.1128/JVI.03399-12.
15. Devaiah, B.N.; Case-Borden, C.; Gegonne, A.; Hsu, C.H.; Chen, Q.; Meerzaman, D.; Dey, A.; Ozato, K.; Singer, D.S. BRD4 is a histone acetyltransferase that evicts nucleosomes from chromatin. *Nat Struct Mol Biol* **2016**, *23*, 540–8. Type: Journal Article, doi:10.1038/nsmb.3228.
16. Wu, T.; Kamikawa, Y.F.; Donohoe, M.E. Brd4's Bromodomains Mediate Histone H3 Acetylation and Chromatin Remodeling in Pluripotent Cells through P300 and Brg1. *Cell Rep* **2018**, *25*, 1756–1771. Type: Journal Article, doi:10.1016/j.celrep.2018.10.003.
17. Karin, M.; Ben-Neriah, Y. Phosphorylation meets ubiquitination: the control of NF-[kappa]B activity. *Annu Rev Immunol* **2000**, *18*, 621–63. Type: Journal Article, doi:10.1146/annurev.immunol.18.1.621.
18. Meier, F.; Beck, S.; Grassl, N.; Lubeck, M.; Park, M.A.; Raether, O.; Mann, M. Parallel Accumulation-Serial Fragmentation (PASEF): Multiplying Sequencing Speed and Sensitivity by Synchronized Scans in a Trapped Ion Mobility Device. *J Proteome Res* **2015**, *14*, 5378–87. Type: Journal Article, doi:10.1021/acs.jproteome.5b00932.
19. Liu, Z.; Tian, B.; Chen, H.; Wang, P.; Brasier, A.R.; Zhou, J. Discovery of potent and selective BRD4 inhibitors capable of blocking TLR3-induced acute airway inflammation. *Eur J Med Chem* **2018**, *151*, 450–461. doi:10.1016/j.ejmech.2018.04.006.
20. Tian, B.; Liu, Z.; Litvinov, J.; Maroto, R.; Jamaluddin, M.; Rytting, E.; Patrikeev, I.; Ochoa, L.; Vargas, G.; Motamedi, M.; Ameredes, B.T.; Zhou, J.; Brasier, A.R. Efficacy of Novel Highly Specific Bromodomain-Containing Protein 4 Inhibitors in Innate Inflammation-Driven Airway Remodeling. *Am J Respir Cell Mol Biol* **2019**, *60*, 68–83. Type: Journal Article, doi:10.1165/rcmb.2017-0445OC.
21. Hu, J.; Tian, C.Q.; Damaneh, M.S.; Li, Y.; Cao, D.; Lv, K.; Yu, T.; Meng, T.; Chen, D.; Wang, X.; Chen, L.; Li, J.; Song, S.S.; Huan, X.J.; Qin, L.; Shen, J.; Wang, Y.Q.; Miao, Z.H.; Xiong, B. Structure-Based Discovery and Development of a Series of Potent and Selective Bromodomain and Extra-Terminal Protein Inhibitors. *J Med Chem* **2019**, *62*, 8642–8663. Type: Journal Article, doi:10.1021/acs.jmedchem.9b01094.
22. Brown, K.A.; Chen, B.; Guardado-Alvarez, T.M.; Lin, Z.; Hwang, L.; Ayaz-Guner, S.; Jin, S.; Ge, Y. A photocleavable surfactant for top-down proteomics. *Nature Methods* **2019**, *16*, 417–420. Number: 5 Publisher: Nature Publishing Group, doi:10.1038/s41592-019-0391-1.
23. Brown, K.A.; Tucholski, T.; Eken, C.; Knott, S.; Zhu, Y.; Jin, S.; Ge, Y. High-Throughput Proteomics Enabled by a Photocleavable Surfactant. *Angewandte Chemie International Edition* **2020**, *59*, 8406–8410. doi:https://doi.org/10.1002/anie.201915374.
24. Tian, B.; Yang, J.; Zhao, Y.; Ivanciuc, T.; Sun, H.; Wakamiya, M.; Garofalo, R.P.; Brasier, A.R. Central Role of the NF- $\kappa$ B Pathway in the Scgb1a1-Expressing Epithelium in Mediating Respiratory Syncytial Virus-Induced Airway Inflammation. *Journal of Virology* **2018**, *92*. Publisher: American Society for Microbiology Journals Section: Cellular Response to Infection, doi:10.1128/JVI.00441-18.
25. Ueba, O. Respiratory syncytial virus. I. Concentration and purification of the infectious virus. *Acta Med Okayama* **1978**, *32*, 265–272.
26. Xu, X.; Qiao, D.; Mann, M.; Garofalo, R.P.; Brasier, A.R. Respiratory Syncytial Virus Infection Induces Chromatin Remodeling to Activate Growth Factor and Extracellular Matrix Secretion Pathways. *Viruses* **2020**, *12*. Type: Journal Article, doi:10.3390/v12080804.
27. Ramirez, R.D.; Sheridan, S.; Girard, L.; Sato, M.; Kim, Y.; Pollack, J.; Peyton, M.; Zou, Y.; Kurie, J.M.; Dimaio, J.M.; Milchgrub, S.; Smith, A.L.; Souza, R.F.; Gilbey, L.; Zhang, X.; Gandia, K.; Vaughan, M.B.; Wright, W.E.; Gazdar, A.F.; Shay, J.W.; Minna, J.D. Immortalization of human bronchial epithelial cells in the absence of viral oncoproteins. *Cancer Res* **2004**, *64*, 9027–34. Type: Journal Article, doi:10.1158/0008-5472.CAN-04-3703.
28. Ijaz, T.; Pazdrak, K.; Kalita, M.; Konig, R.; Choudhary, S.; Tian, B.; Boldogh, I.; Brasier, A.R. Systems biology approaches to understanding Epithelial Mesenchymal Transition (EMT) in mucosal remodeling and signaling in asthma. *World Allergy Organ J* **2014**, *7*, 13. Type: Journal Article, doi:10.1186/1939-4551-7-13.
29. Tian, B.; Patrikeev, I.; Ochoa, L.; Vargas, G.; Belanger, K.K.; Litvinov, J.; Boldogh, I.; Ameredes, B.T.; Motamedi, M.; Brasier, A.R. NF- $\kappa$ B Mediates Mesenchymal Transition, Remodeling, and Pulmonary Fibrosis in Response to Chronic Inflammation by Viral RNA Patterns. *Am J Respir Cell Mol Biol* **2017**, *56*, 506–520. Type: Journal Article, doi:10.1165/rcmb.2016-0259OC.
30. Zhang, Y.; Sun, H.; Zhang, J.; Brasier, A.R.; Zhao, Y. Quantitative Assessment of the Effects of Trypsin Digestion Methods on Affinity Purification-Mass Spectrometry-based Protein-Protein Interaction Analysis. *J Proteome Res* **2017**, *16*, 3068–3082. Type: Journal Article, doi:10.1021/acs.jproteome.7b00432.
31. Cox, J.; Mann, M. MaxQuant enables high peptide identification rates, individualized p.p.b.-range mass accuracies and proteome-wide protein quantification. *Nature Biotechnology* **2008**, *26*, 1367–1372. Number: 12 Publisher: Nature Publishing Group, doi:10.1038/nbt.1511.

32. Cox, J.; Hein, M.Y.; Lubner, C.A.; Paron, I.; Nagaraj, N.; Mann, M. Accurate Proteome-wide Label-free Quantification by Delayed Normalization and Maximal Peptide Ratio Extraction, Termed MaxLFQ \*. *Molecular & Cellular Proteomics* **2014**, *13*, 2513–2526. Publisher: Elsevier, doi:10.1074/mcp.M113.031591.
33. Wieczorek, S.; Combes, F.; Lazar, C.; Giai Gianetto, Q.; Gatto, L.; Dorffer, A.; Hesse, A.M.; Couté, Y.; Ferro, M.; Bruley, C.; Burger, T. DAPAR & ProStaR: software to perform statistical analyses in quantitative discovery proteomics. *Bioinformatics* **2017**, *33*, 135–136. doi:10.1093/bioinformatics/btw580.
34. R Core Team. *R: A Language and Environment for Statistical Computing*; R Foundation for Statistical Computing: Vienna, Austria, 2020.
35. Pino, L.K.; Searle, B.C.; Bollinger, J.G.; Nunn, B.; MacLean, B.; MacCoss, M.J. The Skyline ecosystem: Informatics for quantitative mass spectrometry proteomics. *Mass Spectrom Rev* **2020**, *39*, 229–244. doi:10.1002/mas.21540.
36. Wickham, H. *ggplot2: Elegant Graphics for Data Analysis*; Springer-Verlag New York, 2016.
37. Kassambara, A. *ggpubr: 'ggplot2' Based Publication Ready Plots*, 2020.
38. Chen, H. *VennDiagram: Generate High-Resolution Venn and Euler Plots*, 2018.
39. Neuwirth, E. *RColorBrewer: ColorBrewer Palettes*, 2014.
40. Thomas, P.D.; Campbell, M.J.; Kejariwal, A.; Mi, H.; Karlak, B.; Daverman, R.; Diemer, K.; Muruganujan, A.; Narechania, A. PANTHER: A Library of Protein Families and Subfamilies Indexed by Function. *Genome Res.* **2003**, *13*, 2129–2141. Company: Cold Spring Harbor Laboratory Press Distributor: Cold Spring Harbor Laboratory Press Institution: Cold Spring Harbor Laboratory Press Label: Cold Spring Harbor Laboratory Press Publisher: Cold Spring Harbor Lab, doi:10.1101/gr.772403.
41. Thomas, P.D.; Kejariwal, A.; Guo, N.; Mi, H.; Campbell, M.J.; Muruganujan, A.; Lazareva-Ulitsky, B. Applications for protein sequence–function evolution data: mRNA/protein expression analysis and coding SNP scoring tools. *Nucleic Acids Research* **2006**, *34*, W645–W650. doi:10.1093/nar/gkl229.
42. Szklarczyk, D.; Gable, A.L.; Lyon, D.; Junge, A.; Wyder, S.; Huerta-Cepas, J.; Simonovic, M.; Doncheva, N.T.; Morris, J.H.; Bork, P.; Jensen, L.J.; Mering, C.v. STRING v11: protein-protein association networks with increased coverage, supporting functional discovery in genome-wide experimental datasets. *Nucleic Acids Res* **2019**, *47*, D607–D613. doi:10.1093/nar/gky1131.
43. Ahlmann-Eltze, C. *ggupset: Combination Matrix Axis for 'ggplot2' to Create 'UpSet' Plots*, 2020.
44. Shannon, P.; Markiel, A.; Ozier, O.; Baliga, N.S.; Wang, J.T.; Ramage, D.; Amin, N.; Schwikowski, B.; Ideker, T. Cytoscape: a software environment for integrated models of biomolecular interaction networks. *Genome Res* **2003**, *13*, 2498–2504. doi:10.1101/gr.1239303.
45. Doncheva, N.T.; Morris, J.H.; Gorodkin, J.; Jensen, L.J. Cytoscape StringApp: Network Analysis and Visualization of Proteomics Data. *J Proteome Res* **2019**, *18*, 623–632. doi:10.1021/acs.jproteome.8b00702.
46. Morris, J.H.; Apeltsin, L.; Newman, A.M.; Baumbach, J.; Wittkop, T.; Su, G.; Bader, G.D.; Ferrin, T.E. clusterMaker: a multi-algorithm clustering plugin for Cytoscape. *BMC Bioinformatics* **2011**, *12*, 436. doi:10.1186/1471-2105-12-436.
47. Lieber, M.; Smith, B.; Szakal, A.; Nelson-Rees, W.; Todaro, G. A continuous tumor-cell line from a human lung carcinoma with properties of type II alveolar epithelial cells. *Int J Cancer* **1976**, *17*, 62–70. Type: Journal Article, doi:10.1002/ijc.2910170110.
48. Foster, K.A.; Oster, C.G.; Mayer, M.M.; Avery, M.L.; Audus, K.L. Characterization of the A549 cell line as a type II pulmonary epithelial cell model for drug metabolism. *Exp Cell Res* **1998**, *243*, 359–66. Type: Journal Article, doi:10.1006/excr.1998.4172.
49. Ijaz, T.; Jamaluddin, M.; Zhao, Y.; Zhang, Y.; Jay, J.; Finnerty, C.C.; Herndon, D.N.; Tilton, R.G.; Brasier, A.R. Coordinate activities of BRD4 and CDK9 in the transcriptional elongation complex are required for TGFβ-induced Nox4 expression and myofibroblast transdifferentiation. *Cell Death Dis* **2017**, *8*, e2606. Type: Journal Article, doi:10.1038/cddis.2016.434.
50. Bösen, C.A.; Farnung, L.; Hintermair, C.; Merzel Schachter, M.; Vogel-Bachmayr, K.; Blazek, D.; Anand, K.; Fisher, R.P.; Eick, D.; Geyer, M. The structure and substrate specificity of human Cdk12/Cyclin K. *Nature Communications* **2014**, *5*, 3505. Number: 1 Publisher: Nature Publishing Group, doi:10.1038/ncomms4505.
51. Liang, K.; Gao, X.; Gilmore, J.M.; Florens, L.; Washburn, M.P.; Smith, E.; Shilatifard, A. Characterization of human cyclin-dependent kinase 12 (CDK12) and CDK13 complexes in C-terminal domain phosphorylation, gene transcription, and RNA processing. *Mol Cell Biol* **2015**, *35*, 928–938. doi:10.1128/MCB.01426-14.
52. Zenz, R.; Wagner, E.F. Jun signalling in the epidermis: From developmental defects to psoriasis and skin tumors. *The International Journal of Biochemistry & Cell Biology* **2006**, *38*, 1043–1049. doi:10.1016/j.biocel.2005.11.011.
53. Wagner, E.F. Bone development and inflammatory disease is regulated by AP-1 (Fos/Jun). *Annals of the Rheumatic Diseases* **2010**, *69*, i86–i88. Publisher: BMJ Publishing Group Ltd Section: Papers, doi:10.1136/ard.2009.119396.
54. Khalaf, H.; Jass, J.; Olsson, P.E. Differential cytokine regulation by NF-kappaB and AP-1 in Jurkat T-cells. *BMC Immunol* **2010**, *11*, 26. doi:10.1186/1471-2172-11-26.
55. Larhammar, M.; Huntwork-Rodriguez, S.; Rudhard, Y.; Sengupta-Ghosh, A.; Lewcock, J.W. The Ste20 Family Kinases MAP4K4, MINK1, and TNIK Converge to Regulate Stress-Induced JNK Signaling in Neurons. *J Neurosci* **2017**, *37*, 11074–11084. doi:10.1523/JNEUROSCI.0905-17.2017.
56. Addison, W.N.; Pellicelli, M.; St-Arnaud, R. Dephosphorylation of the transcriptional cofactor NACA by the PP1A phosphatase enhances cJUN transcriptional activity and osteoblast differentiation. *J Biol Chem* **2019**, *294*, 8184–8196. doi:10.1074/jbc.RA118.006920.

57. Rahman, S.; Sowa, M.E.; Ottinger, M.; Smith, J.A.; Shi, Y.; Harper, J.W.; Howley, P.M. The Brd4 Extraterminal Domain Confers Transcription Activation Independent of pTEFb by Recruiting Multiple Proteins, Including NSD3. *Molecular and Cellular Biology* **2011**, *31*, 2641–2652. Publisher: American Society for Microbiology Journals Section: Articles, doi:10.1128/MCB.01341-10.
58. Toualbi, K.; Güller, M.C.; Mauriz, J.L.; Labalette, C.; Buendia, M.A.; Mauviel, A.; Bernuau, D. Physical and functional cooperation between AP-1 and  $\beta$ -catenin for the regulation of TCF-dependent genes. *Oncogene* **2007**, *26*, 3492–3502. Number: 24 Publisher: Nature Publishing Group, doi:10.1038/sj.onc.1210133.
59. Xiao, W.; Hodge, D.R.; Wang, L.; Yang, X.; Zhang, X.; Farrar, W.L. NF-kappaB activates IL-6 expression through cooperation with c-Jun and IL6-AP1 site, but is independent of its IL6-NFkappaB regulatory site in autocrine human multiple myeloma cells. *Cancer Biol Ther* **2004**, *3*, 1007–1017. doi:10.4161/cbt.3.10.1141.
60. Lever, A.R.; Park, H.; Mulhern, T.J.; Jackson, G.R.; Comolli, J.C.; Borenstein, J.T.; Hayden, P.J.; Prantil-Baun, R. Comprehensive evaluation of poly(I:C) induced inflammatory response in an airway epithelial model. *Physiol Rep* **2015**, *3*. doi:10.14814/phy2.12334.
61. Aeffer, F.; Traylor, Z.P.; Yu, E.N.Z.; Davis, I.C. Double-stranded RNA induces similar pulmonary dysfunction to respiratory syncytial virus in BALB/c mice. *Am J Physiol Lung Cell Mol Physiol* **2011**, *301*, L99–L109. doi:10.1152/ajplung.00398.2010.
62. Dunham, W.H.; Mullin, M.; Gingras, A.C. Affinity-purification coupled to mass spectrometry: Basic principles and strategies. *PROTEOMICS* **2012**, *12*, 1576–1590. eprint: <https://onlinelibrary.wiley.com/doi/pdf/10.1002/pmic.201100523>, doi:<https://doi.org/10.1002/pmic.201100523>.
63. Morris, J.H.; Knudsen, G.M.; Verschueren, E.; Johnson, J.R.; Cimermancic, P.; Greninger, A.L.; Pico, A.R. Affinity purification–mass spectrometry and network analysis to understand protein–protein interactions. *Nat Protoc* **2014**, *9*, 2539–2554. doi:10.1038/nprot.2014.164.
64. Rauniyar, N.; Yates, J.R. Isobaric Labeling-Based Relative Quantification in Shotgun Proteomics. *J Proteome Res* **2014**, *13*, 5293–5309. doi:10.1021/pr500880b.
65. Tate, S.; Larsen, B.; Bonner, R.; Gingras, A.C. Label-free quantitative proteomics trends for protein–protein interactions. *Journal of Proteomics* **2013**, *81*, 91–101. doi:10.1016/j.jpro.2012.10.027.
66. Dawson, M.A.; Prinjha, R.K.; Dittman, A.; Giotopoulos, G.; Bantscheff, M.; Chan, W.I.; Robson, S.C.; Chung, C.w.; Hopf, C.; Savitski, M.M.; Huthmacher, C.; Gudgin, E.; Lugo, D.; Beinke, S.; Chapman, T.D.; Roberts, E.J.; Soden, P.E.; Auger, K.R.; Mirguet, O.; Doehner, K.; Delwel, R.; Burnett, A.K.; Jeffrey, P.; Drewes, G.; Lee, K.; Huntly, B.J.; Kouzarides, T. Inhibition of BET recruitment to chromatin as an effective treatment for MLL-fusion leukaemia. *Nature* **2011**, *478*, 529–533. doi:10.1038/nature10509.
67. Hoffmann, A.; Natoli, G.; Ghosh, G. Transcriptional regulation via the NF-kappaB signaling module. *Oncogene* **2006**, *25*, 6706–16. Type: Journal Article, doi:10.1038/sj.onc.1209933.
68. Sen, R.; Smale, S.T. Selectivity of the NF-kappaB response. *Cold Spring Harb Perspect Biol* **2010**, *2*, a000257. Type: Journal Article, doi:10.1101/cshperspect.a000257.
69. Zhao, M.; Joy, J.; Zhou, W.; De, S.; Wood, W.H.; Becker, K.G.; Ji, H.; Sen, R. Transcriptional outcomes and kinetic patterning of gene expression in response to NF- $\kappa$ B activation. *PLoS Biol* **2018**, *16*, e2006347. Type: Journal Article, doi:10.1371/journal.pbio.2006347.
70. Alsarraj, J.; Faraji, F.; Geiger, T.R.; Mattaini, K.R.; Williams, M.; Wu, J.; Ha, N.H.; Merlino, T.; Walker, R.C.; Bosley, A.D.; Xiao, Z.; Andresson, T.; Esposito, D.; Smithers, N.; Lugo, D.; Prinjha, R.; Day, A.; Crawford, N.P.S.; Ozato, K.; Gardner, K.; Hunter, K.W. BRD4 Short Isoform Interacts with RRP1B, SIPA1 and Components of the LINC Complex at the Inner Face of the Nuclear Membrane. *PLOS ONE* **2013**, *8*, e80746. Publisher: Public Library of Science, doi:10.1371/journal.pone.0080746.
71. Jung, M.; Philpott, M.; Müller, S.; Schulze, J.; Badock, V.; Eberspächer, U.; Moosmayer, D.; Bader, B.; Schmees, N.; Fernández-Montalván, A.; Haendler, B. Affinity Map of Bromodomain Protein 4 (BRD4) Interactions with the Histone H4 Tail and the Small Molecule Inhibitor JQ1. *J Biol Chem* **2014**, *289*, 9304–9319. doi:10.1074/jbc.M113.523019.
72. Tian, B.; Zhao, Y.; Sun, H.; Zhang, Y.; Yang, J.; Brasier, A.R. BRD4 mediates NF- $\kappa$ B-dependent epithelial-mesenchymal transition and pulmonary fibrosis via transcriptional elongation. *American Journal of Physiology-Lung Cellular and Molecular Physiology* **2016**, *311*, L1183–L1201. Publisher: American Physiological Society, doi:10.1152/ajplung.00224.2016.
73. Xiang, N.; He, M.; Ishaq, M.; Gao, Y.; Song, F.; Guo, L.; Ma, L.; Sun, G.; Liu, D.; Guo, D.; Chen, Y. The DEAD-Box RNA Helicase DDX3 Interacts with NF- $\kappa$ B Subunit p65 and Suppresses p65-Mediated Transcription. *PLoS One* **2016**, *11*. doi:10.1371/journal.pone.0164471.
74. Fullam, A.; Gu, L.; Höhn, Y.; Schröder, M. DDX3 directly facilitates IKK $\alpha$  activation and regulates downstream signalling pathways. *Biochemical Journal* **2018**, *475*, 3595–3607. doi:10.1042/BCJ20180163.
75. Rong, C.; Shi, Y.; Huang, J.; Wang, X.; Shimizu, R.; Mori, Y.; Murai, A.; Liang, J. The Effect of Metadherin on NF- $\kappa$ B Activation and Downstream Genes in Ovarian Cancer. *Cell Transplant* **2020**, *29*. doi:10.1177/0963689720905506.
76. Bhatt, D.; Ghosh, S. Regulation of the NF- $\kappa$ B-Mediated Transcription of Inflammatory Genes. *Front. Immunol.* **2014**, *5*. Publisher: Frontiers, doi:10.3389/fimmu.2014.00071.
77. Shaulian, E.; Karin, M. AP-1 as a regulator of cell life and death. *Nature Cell Biology* **2002**, *4*, E131–E136. Number: 5 Publisher: Nature Publishing Group, doi:10.1038/ncb0502-e131.
78. Yang, J.; Mitra, A.; Dojer, N.; Fu, S.; Rowicka, M.; Brasier, A.R. A probabilistic approach to learn chromatin architecture and accurate inference of the NF- $\kappa$ B/RelA regulatory network using ChIP-Seq. *Nucleic Acids Res* **2013**, *41*, 7240–7259. doi:10.1093/nar/gkt493.
79. Du, Q.; Geller, D.A. Cross-Regulation Between Wnt and NF- $\kappa$ B Signaling Pathways. *For Immunopathol Dis Therap* **2010**, *1*, 155–181. doi:10.1615/ForumImmunDisTher.v1.i3.

80. Ma, B.; Hottiger, M.O. Crosstalk between Wnt/ $\beta$ -Catenin and NF- $\kappa$ B Signaling Pathway during Inflammation. *Front Immunol* **2016**, *7*. doi:10.3389/fimmu.2016.00378.
81. Jia, D.; Yang, W.; Li, L.; Liu, H.; Tan, Y.; Ooi, S.; Chi, L.; Filion, L.G.; Figeys, D.; Wang, L.  $\beta$ -Catenin and NF- $\kappa$ B co-activation triggered by TLR3 stimulation facilitates stem cell-like phenotypes in breast cancer. *Cell Death & Differentiation* **2015**, *22*, 298–310. Number: 2 Publisher: Nature Publishing Group, doi:10.1038/cdd.2014.145.
82. Deng, J.; Miller, S.A.; Wang, H.Y.; Xia, W.; Wen, Y.; Zhou, B.P.; Li, Y.; Lin, S.Y.; Hung, M.C.  $\beta$ -catenin interacts with and inhibits NF- $\kappa$ B in human colon and breast cancer. *Cancer Cell* **2002**, *2*, 323–334. doi:10.1016/S1535-6108(02)00154-X.
83. Valenta, T.; Hausmann, G.; Basler, K. The many faces and functions of  $\beta$ -catenin. *EMBO J* **2012**, *31*, 2714–2736. doi:10.1038/emboj.2012.150.
84. Bottomly, D.; Kyler, S.L.; McWeeney, S.K.; Yochum, G.S. Identification of  $\beta$ -catenin binding regions in colon cancer cells using ChIP-Seq. *Nucleic Acids Res* **2010**, *38*, 5735–5745. doi:10.1093/nar/gkq363.
85. Filippakopoulos, P.; Qi, J.; Picaud, S.; Shen, Y.; Smith, W.B.; Fedorov, O.; Morse, E.M.; Keates, T.; Hickman, T.T.; Felletar, I.; Philpott, M.; Munro, S.; McKeown, M.R.; Wang, Y.; Christie, A.L.; West, N.; Cameron, M.J.; Schwartz, B.; Heightman, T.D.; La Thangue, N.; French, C.A.; Wiest, O.; Kung, A.L.; Knapp, S.; Bradner, J.E. Selective inhibition of BET bromodomains. *Nature* **2010**, *468*, 1067–1073. doi:10.1038/nature09504.
86. Doroshow, D.B.; Eder, J.P.; LoRusso, P.M. BET inhibitors: a novel epigenetic approach. *Annals of Oncology* **2017**, *28*, 1776–1787. Publisher: Elsevier, doi:10.1093/annonc/mdx157.
87. Jiang, Y.G.; Luo, Y.; He, D.L.; Li, X.; Zhang, L.L.; Peng, T.; Li, M.C.; Lin, Y.H. Role of Wnt/ $\beta$ -catenin signaling pathway in epithelial-mesenchymal transition of human prostate cancer induced by hypoxia-inducible factor-1 $\alpha$ . *International Journal of Urology* **2007**, *14*, 1034–1039. eprint: <https://onlinelibrary.wiley.com/doi/pdf/10.1111/j.1442-2042.2007.01866.x>, doi:<https://doi.org/10.1111/j.1442-2042.2007.01866.x>.
88. Will, C.L.; Lührmann, R. Spliceosome Structure and Function. *Cold Spring Harb Perspect Biol* **2011**, *3*. doi:10.1101/cshperspect.a003707.
89. Jarnæss, E.; Stokka, A.J.; Kvissel, A.K.; Skålhegg, B.S.; Torgersen, K.M.; Scott, J.D.; Carlson, C.R.; Taskén, K. Splicing Factor Arginine/Serine-rich 17A (SFRS17A) Is an A-kinase Anchoring Protein That Targets Protein Kinase A to Splicing Factor Compartments. *J Biol Chem* **2009**, *284*, 35154–35164. doi:10.1074/jbc.M109.056465.
90. Taylor, D.J.; Devkota, B.; Huang, A.D.; Topf, M.; Narayanan, E.; Sali, A.; Harvey, S.C.; Frank, J. Comprehensive Molecular Structure of the Eukaryotic Ribosome. *Structure* **2009**, *17*, 1591. doi:10.1016/j.str.2009.09.015.
91. Jackson, R.J.; Hellen, C.U.; Pestova, T.V. THE MECHANISM OF EUKARYOTIC TRANSLATION INITIATION AND PRINCIPLES OF ITS REGULATION. *Nat Rev Mol Cell Biol* **2010**, *11*, 113–127. doi:10.1038/nrm2838.
92. Grantham, J. The Molecular Chaperone CCT/TRiC: An Essential Component of Proteostasis and a Potential Modulator of Protein Aggregation. *Front. Genet.* **2020**, *11*. Publisher: Frontiers, doi:10.3389/fgene.2020.00172.
93. Linxweiler, M.; Schick, B.; Zimmermann, R. Let's talk about Secs: Sec61, Sec62 and Sec63 in signal transduction, oncology and personalized medicine. *Signal Transduction and Targeted Therapy* **2017**, *2*, 1–10. Number: 1 Publisher: Nature Publishing Group, doi:10.1038/sigtrans.2017.2.
94. Rosonina, E.; Blencowe, B.J. Gene Expression: The Close Coupling of Transcription and Splicing. *Current Biology* **2002**, *12*, R319–R321. Publisher: Elsevier, doi:10.1016/S0960-9822(02)00829-1.
95. Aviner, R.; Hofmann, S.; Elman, T.; Shenoy, A.; Geiger, T.; Elkon, R.; Ehrlich, M.; Elroy-Stein, O. Proteomic analysis of polyribosomes identifies splicing factors as potential regulators of translation during mitosis. *Nucleic Acids Res* **2017**, *45*, 5945–5957. doi:10.1093/nar/gkx326.
96. Palangat, M.; Anastakis, D.G.; Fei, D.L.; Lindblad, K.E.; Bradley, R.; Hourigan, C.S.; Hafner, M.; Larson, D.R. The splicing factor U2AF1 contributes to cancer progression through a noncanonical role in translation regulation. *Genes Dev* **2019**, *33*, 482–497. doi:10.1101/gad.319590.118.
97. Perez-Riverol, Y.; Csordas, A.; Bai, J.; Bernal-Llinares, M.; Hewapathirana, S.; Kundu, D.J.; Inuganti, A.; Griss, J.; Mayer, G.; Eisenacher, M.; Pérez, E.; Uszkoreit, J.; Pfeuffer, J.; Sachsenberg, T.; Yilmaz, Ş.; Tiwary, S.; Cox, J.; Audain, E.; Walzer, M.; Jarnuczak, A.F.; Ternent, T.; Brazma, A.; Vizcaíno, J.A. The PRIDE database and related tools and resources in 2019: improving support for quantification data. *Nucleic Acids Res* **2019**, *47*, D442–D450. doi:10.1093/nar/gky1106.